




Special Issue on Selected Emerging Trends in Terahertz Science and Technology

Terahertz Quantum-Cascade Lasers: From Design to Applications

Xiang Lü , Benjamin Röben , Valentino Pistori , Klaus Biermann , Esperanza Luna , Martin Wienold , Heinz-Wilhelm Hübers , Jente R. Wubs , Jean-Pierre H. van Helden , Pierre Gellie, and Lutz Schrottke 

Abstract—We report on the development and the application of high-performance terahertz (THz) quantum-cascade lasers (QCLs) based on GaAs/Al_xGa_{1-x}As heterostructures. These lasers with emission frequencies between 2.6 and 4.7 THz are based on a hybrid design, which is preferred for continuous-wave applications. For the design of the active regions, we employ an efficient Fourier-transform-based model, which also allows for the simulation of heterostructures with gradual interfaces. Since the inherent interface width is on the same order as the thickness of the layers in the active region, the use of nominally binary AlAs barriers results in an effective Al content up to $x = 0.6$ for the tallest barriers. For practical applications, Fabry–Pérot lasers based on single-plasmon waveguides are fabricated. Single-mode operation is in most cases achieved by using short cavities. In particular, GaAs/AlAs THz QCLs show a sufficiently high wall plug efficiency so that they can be operated in miniature mechanical cryocoolers. Currently, high-performance THz QCLs are used for commercial continuous-wave, table-top THz systems, local oscillators in 3.5- and 4.7-THz heterodyne spectrometers, and absorption spectrometers for the determination of the density of atomic oxygen in plasmas.

Index Terms—High-resolution spectroscopy, quantum-cascade laser (QCL), terahertz (THz) spectroscopy.

I. INTRODUCTION

ALMOST 30 years ago, a new type of semiconductor laser, the quantum-cascade laser (QCL), was invented [1]. In contrast to conventional interband semiconductor lasers, the lasing transitions in QCLs are intersubband transitions within the conduction or valence band rather than across the energy gap. Therefore, QCLs are unipolar lasers, i.e., only one type of carrier, typically electrons, is injected into the laser structure. In order to obtain population inversion between the subbands, rather complex semiconductor heterostructures are employed.

While the first QCLs emitted light in the mid-infrared spectral region, a QCL for the terahertz (THz) spectral region was reported in 2002 [2]. The THz spectral region, which typically covers the range from 0.1 to 10 THz, bridges the electronics-based microwave region with the optics-based infrared region. Despite the strong interest in the THz region, there is still a lack of compact, powerful radiation sources, the so-called THz gap, which can be filled by powerful THz QCLs. Their active regions consist of modules with 4–20 layers with thicknesses on the order of several nanometers [3], [4], [5], which are repeated about 100 times, so that the total thickness of the complete structures typically amounts to about 10 μm . The excellent state of semiconductor science and technology allows for the development and fabrication of those sophisticated devices, which rely on the high-quality growth of complex planar heterostructures using molecular beam epitaxy (MBE) and the comprehensive understanding of the physical processes in them.

There are two basic types of active regions for THz QCLs. In the so-called bound-to-continuum (BTC) design, the upper laser level is a more or less bound state, whereas the lower laser level is embedded in a quasi-miniband [6]. The second design is the so-called resonant-phonon (RP) design, in which a very fast transition resonant to the energy of the longitudinal optical (LO) phonon depletes the lower laser level and injects carriers into the upper laser level of the following unit cell [7], [8]. A combination of the BTC design with the RP design, a

Manuscript received 31 January 2024; revised 14 May 2024; accepted 8 June 2024. Date of publication 17 June 2024; date of current version 5 September 2024. This work was supported in part by European Space Agency through Subcontract D/973/67268909 under ESA Grant 4000125911/18/NL/AF, in part by Leibniz-Gemeinschaft under Grant K54/2017, and in part by Deutsche Forschungsgemeinschaft (DFG, German Research Foundation) under Grant 468535812. (Corresponding author: Xiang Lü.)

Xiang Lü, Valentino Pistori, Klaus Biermann, Esperanza Luna, and Lutz Schrottke are with the Paul-Drude-Institut für Festkörperelektronik, Leibniz-Institut im Forschungsverbund Berlin e. V., 10117 Berlin, Germany (e-mail: lue@pdi-berlin.de; pistori@pdi-berlin.de; biermann@pdi-berlin.de; luna@pdi-berlin.de; lutz@pdi-berlin.de).

Benjamin Röben is with the Physikalisch-Technische Bundesanstalt, Institut Berlin, 10587 Berlin, Germany (e-mail: benjamin.roeben@ptb.de).

Martin Wienold is with the German Aerospace Center (DLR), Institute of Optical Sensor Systems, 12489 Berlin, Germany (e-mail: martin.wienold@dlr.de).

Heinz-Wilhelm Hübers is with the German Aerospace Center (DLR), Institute of Optical Sensor Systems, 12489 Berlin, Germany, and also with the Department of Physics, Humboldt-Universität zu Berlin, 12489 Berlin, Germany (e-mail: heinz-wilhelm.huebers@dlr.de).

Jente R. Wubs and Jean-Pierre H. van Helden are with the Leibniz Institute for Plasma Science and Technology (INP), 17489 Greifswald, Germany (e-mail: jente.wubs@inp-greifswald.de; jean-pierre.vanhelden@inp-greifswald.de).

Pierre Gellie is with the Lytid SAS, 91400 Orsay, France (e-mail: p.gellie@lytid.com).

Color versions of one or more figures in this article are available at <https://doi.org/10.1109/TTHZ.2024.3415501>.

Digital Object Identifier 10.1109/TTHZ.2024.3415501

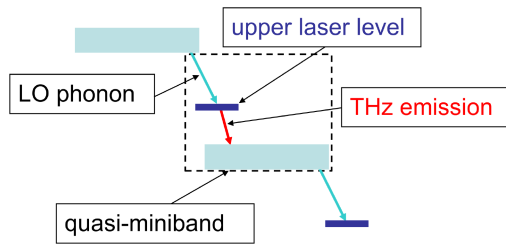


Fig. 1. Schematic representation of a hybrid design for a THz QCL. The dashed-line rectangle indicates a single stage.

so-called hybrid design [9], [10], [11], may allow for rather large optical gain at comparatively low pumping power. Here, the lasing transition is from a more or less localized state to a quasi-miniband, which in turn is coupled to a transition resonant to the LO phonon energy, as shown in Fig. 1. Its rather large gain at moderate pumping powers makes this design attractive for continuous-wave (cw) operation in coolant-free mechanical cryocoolers and hence for practical applications [12].

For the simulation of THz QCLs, theoretical models with different levels of complexity and computational cost were developed. However, for practical design purposes, a scattering-rate method based on the self-consistent solution of the Schrödinger and Poisson equations proves very useful. The self-consistent procedure includes the determination of the scattering rates, which allows for the calculation of the carrier distribution and the Coulomb potential. Using the corrected potential, the equations are solved again until successful convergence is achieved [13]. We developed an efficient and fast phenomenological method in which all components are formulated in the Fourier space [14], [15]. The typical computation time for complete current density-field strength characteristics and the corresponding gain maps amounts to only several minutes.

Since in principle any materials system that allows for the formation of a semiconductor heterostructure could be applied for THz QCLs, several materials combinations, such as GaAs/(Al,Ga)As [2], (In,Ga)As/Ga(As,Sb) [16], and InAs/Al(As,Sb) heterostructures [17] have been explored. However, GaAs/(Al,Ga)As THz QCLs are currently the system of choice, since they can be grown by MBE with extraordinary quality, and the material parameters that are decisive for the design of THz QCLs are precisely known. As an additional degree of freedom, this materials system allows for any nominal composition of the $\text{Al}_x\text{Ga}_{1-x}\text{As}$ barriers with $0 \leq x \leq 1$ leading to conduction band offsets at Γ point between 0 and about 980 meV although the actual value for x in the thin barriers in THz QCLs is still below 1 due to the inherent interface width.

The selection rules for intersubband transitions require the electric field component of the emitted light to be in the growth direction, i.e., the radiation is in-plane. To form a resonator, the THz light has to be guided by a waveguide, for which two types have been developed, namely, the single-plasmon (SP) and the metal–metal (MM) waveguides, as shown in Fig. 2. After MBE growth, the wafers are processed using wet chemical or dry etching. For the most straightforward case, the cleaved facets at both ends of the waveguide are the mirrors of a Fabry–Pérot (FP) resonator. More complex resonator structures, such as lateral

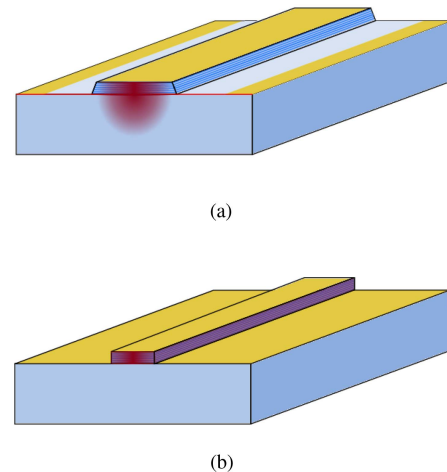


Fig. 2. Schematic representations of (a) the SP waveguide, where the mode is weakly confined between the upper metal contact and a highly doped GaAs layer, which serves at the same time as the bottom contact, and penetrates substantially into the substrate and (b) the MM waveguide, where the mode is confined between two metal layers. Typical dimensions of the laser ridges using SP waveguide are widths of 15–200 μm and lengths of 0.5–7.5 mm.

distributed-feedback gratings [18], [19], antenna coupling [20], and antenna-coupled distributed-feedback gratings [7], [21], have been reported.

SP waveguides allow for FP resonators with reasonable out-coupling efficiency and rather low beam divergence ($\sim 30^\circ$), but they require active regions with rather large optical gain as the overlap between the active region and the waveguide mode, i.e., the confinement factor, is typically below 0.5 depending on the emission frequency and laser geometry. Its value may vary between about 0.2 and about 0.5. While THz QCLs based on RP designs and MM waveguides, which exhibit a larger confinement factor at the expense of a reduced out-coupling, are employed for high-temperature (pulsed) operation, lasers based on hybrid designs and SP waveguides are often advantageous for practical applications that require cw operation. In particular, they allow for a rather straightforward fabrication and exhibit a favorable outcoupling characteristic. For an overview on the design and waveguide types, we refer to [22]. To realize single-mode operation, distributed-feedback lasers using lateral gratings of different order [23], [24], [25], two-section cavity lasers [26], [27], or very short FP cavities are employed [28].

The output power of THz QCLs decreases with increasing heat sink temperature. Therefore, they have to be operated at cryogenic temperatures. However, lasers with sufficiently low pumping power allow for the use of coolant-free mechanical coolers. The detailed understanding of the physical processes essential for the temperature dependence of the operating properties as well as the increase of the operating temperatures for both pulsed and cw operation is subject to current research.

The cw operation of THz QCLs with typical output powers from several mW to tens of mW in mechanical cryocoolers or even in miniature coolers (cf., Fig. 3) allows for the development of table-top THz radiation sources. The easy use of such systems makes them also very attractive for commercial systems, which have been employed in many experimental setups since

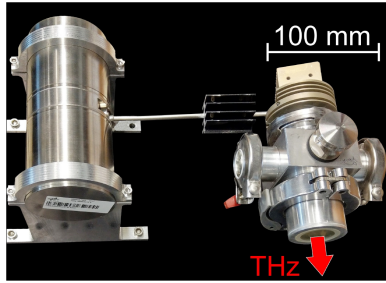


Fig. 3. Miniature cooler (AIM SL400). The red arrow indicates the direction of the THz beam.

they are the only compact, practical, and stable cw radiation source in the range between 2 and 5 THz. For instance, THz QCLs have established themselves as excellent sources for THz detector characterization at the basic-science level, including the exploration of new physical phenomena or materials, such as optomechanics or graphene, for THz detection [29], [30] as well as THz real-time imaging and THz sensing [31], [32], [33]. Furthermore, frequency combs based on THz QCLs [34], [35], [36] operated in a wide frequency range allow for broadband spectroscopy. Self-detection near-field optical microscopy is employed for phase-resolved THz nanoimaging with high resolution far beyond the diffraction limit [37], [38].

The THz region is of particular interest for spectroscopic applications, since rotational states of many molecules, impurity transitions in semiconductors, and fine-structure transitions in atoms as well as ions can result in THz absorption or emission [39]. THz QCLs exhibit extremely narrow emission lines. Therefore, table-top systems based on THz QCLs are also excellent radiation sources for high-resolution heterodyne or absorption spectroscopy, which is difficult to achieve using other radiation sources. THz high-resolution spectroscopy enables new observations in astronomy and atmospheric research, for instance, the detection of atomic oxygen by heterodyne spectroscopy. Furthermore, it allows for the development of novel approaches for plasma diagnostics, such as the precise determination of the absolute density of atoms and ions in technologically relevant plasma processes by absorption spectroscopy.

For the characterization of THz QCLs with respect to applications, the spectral properties as well as the output power–current density–voltage (L – J – V) characteristics as a function of heat sink temperature are decisive parameters. The spectral properties include the center wavelength of the emission and the number of excited laser modes. In particular, for high-resolution spectroscopy, single-mode operation and, additionally, a certain tuning range are required. The lasing spectra are determined using Fourier-transform infrared (FTIR) spectrometers. Although FTIR instruments cannot resolve the linewidth of the lasers, which is in the free-running case on the order of a few MHz, they are sufficient for the determination of the number of modes and their center frequencies. The optical power is measured using calibrated power meters, whereas the electrical characterization is carried out with standard laboratory equipment.

The rest of this article is organized as follows. In Section II, we discuss the active regions, the materials system, and fabrication

methods for THz QCLs for practical applications. Sections III–V are devoted to the implementation of THz QCLs in table-top systems and to applications of heterodyne as well as absorption spectroscopy, respectively. Finally, Section VI concludes this article.

II. MODEL, ACTIVE REGIONS, MATERIALS SYSTEM, AND FABRICATION OF THz QCLs FOR APPLICATIONS

A. Model

A model that can be implemented as a design tool for THz QCLs has to combine sufficient predictability with manageable computation times. This is of particular importance for designs with a larger number of quantum wells per period and an accordingly large number of states that have to be taken into account. In general, carrier transport in semiconductor heterostructures can be treated at various levels of complexity and predictability [40] using approaches, such as scattering-rate systems [14], [41], [42], ensemble Monte Carlo methods [43], [44], and nonequilibrium Green’s function formalisms [45], [46], [47], [48]. For the design of THz QCLs, scattering-rate approaches taking into account only the occupation numbers or simplified density matrix methods [49], [50], [51], [52] are preferred since these approaches allow for sufficient accuracy compared with the experimental reproducibility of nominally identical structures with reasonable numerical effort.

We have continually developed and refined a design tool that is based on the self-consistent solution of the Schrödinger and Poisson equations using a rate-equation approach with phenomenological scattering rates. In each step of the self-consistent loop, the form factors for the scattering rates are calculated from the respective solution of the Schrödinger equation. For a precise alignment of the states, the energy dependence of the effective masses due to the nonparabolicity of the band structure is taken into account. Our approach allowed us to maintain the mathematical structure of an eigenvalue problem so that standard linear algebra can be used efficiently [13]. A conversion of the model into a Fourier transform approach accelerated computation by about one order of magnitude [14] and allowed for the simulation of interface grading without any significant additional computation costs [53]. Since the inherent interface width is comparable with the thickness of the layers in the active region, it will impact the resulting potential profile. As a consequence, the calculated subband energies are affected on a similar order of magnitude as by the energy dependence of the effective masses. Therefore, the interface grading affects the emission frequency, the field strength for resonant coupling of subbands, and the formation of the miniband [53].

However, as it is generally the case for rate equation approaches, this method neglects dephasing processes, which leads to an overestimation of the coupling of remote states and to unrealistically large currents and incorrect values for the gain at certain electric field strengths. To compensate for this drawback, our design method relies on the computation of the current density and gain spectra for a larger number of electric field strengths within a few minutes making use of the very fast computation and to evaluate the entire gain map in combination with the shape of the current density–electric field strength curve

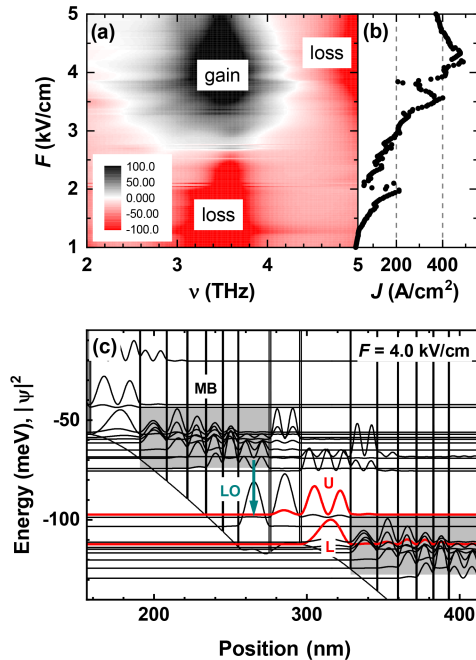


Fig. 4. (a) Calculated gain map as a function of frequency ν and electric field strength F and (b) current density–applied field strength (J – F) characteristics as well as (c) conduction band profile and subband structure of a 3.5-THz GaAs/AlAs QCL. The upper and lower laser levels are marked as U and L , respectively. MB labels the quasi-miniband and LO depicts the transition resonant to the LO phonon.

rather than optimizing gain and current density for a given field strength. Finally, our method may benefit from the future implementation of algorithms of artificial intelligence.

B. Active Regions

For practical applications, in particular for high-resolution spectroscopy, cw operation of THz QCLs in a coolant-free environment is required. Currently, THz QCLs based on the hybrid design are the system of choice if the challenging growth can be handled, since they may provide rather large gain at moderate pumping powers and allow for the implementation of SP waveguides and straightforward FP resonators. The latter eases the practical use of the lasers, in particular, spare lasers may be provided, if necessary, with not too large effort.

Fig. 4 shows (a) the gain spectra as a function of electric field strength F and (b) the current density–electric field strength characteristics (J – F) as well as (c) the subband structure for the 3.5-THz QCL as an example. Note that the accuracy of the actual values for gain and current density should not be overestimated since the calculations are based on phenomenological scattering rates. In our experience, good active-region designs exhibit a rather large field strength range with gain values significantly above the threshold gain, which can be estimated to be about 50 cm^{-1} in this case, and well below the field strength for onset of negative differential conductivity. The dipole matrix elements are rather large due to the vertical lasing transition in our hybrid designs. As an example, the value is about 5.1 nm at 4.0 kV/cm . Note that the values of the dipole matrix elements vary with

increasing field strengths as the coupling of the lower laser level to the quasi-miniband varies.

The complex structure of the active regions does not allow for a straightforward design strategy. In general, any design procedure starts from an initial guess for a layer sequence, for which the electrical and optical properties are simulated and evaluated. Subsequently, the layer sequence is modified and reevaluated. This process is repeated until a design with a satisfactory gain spectrum and level of current density is reached. The comprehensive development cycle includes simulations as well as empirical investigations of lasers fabricated on the basis of the respective simulation results. In some cases, the development of a new design can be started from a well-investigated laser that exhibits operating characteristics similar to the target parameters.

C. Materials System

For THz QCLs, GaAs/Al _{x} Ga _{$1-x$} As heterostructures are the most used materials systems with x ranging from very low values up to nominally $x = 1$. Higher Al content x corresponds to higher barriers in the heterostructures, which are expected to lead to reduced leakage currents. A decade ago, we showed that THz QCLs with nominally binary AlAs barriers exhibit a significant higher wall plug efficiency compared with their GaAs/Al_{0.25}Ga_{0.75}As counterparts due to reduced leakage current and reabsorption [54]. The reduced current density of GaAs/AlAs THz QCLs leads to lower electrical pump power so that cw operation even in miniature coolers is enabled. In order to maintain an efficient resonant tunneling, the AlAs barriers have to be accordingly thin, which imposes also challenges with respect to the growth.

To maintain a high interface quality, rather low growth rates are chosen with typical values for GaAs and AlAs of 0.13 and 0.11 nm/s , respectively. Under these conditions, the tetrameric arsenic (As_4) flux can be kept constant during growth of both alloys. A closed-loop feedback based on the background pressure in the growth chamber is used to keep the arsenic flux constant over the extended growth durations by automatically varying the valve opening of a valved cracker arsenic source. A second automatic closed-loop control based on in situ spectral reflectivity measurements is applied to keep the growth rate constant [55]. The total thickness of the active region of more than $10 \mu\text{m}$ leads to a growth duration of more than 23 h for the active region only.

Intermixing of Ga and Al atoms at the interfaces between quantum wells and barriers leads to a grading of the composition rather than an abrupt interface [56], [57]. Since the interface width of several monolayers is on the same order as the thickness of the barriers in GaAs/AlAs THz QCLs, the actual composition of the barriers may not reach the binary AlAs but a maximum composition value of about 0.6 even for the thickest barriers. The experimental Al composition profile of a QCL structure can be obtained from the analysis of the intensity profile derived from a corresponding g_{002} dark-field transmission electron microscopy (DFTEM) image, which is highly sensitive to variations in the chemistry of the alloy in semiconductors

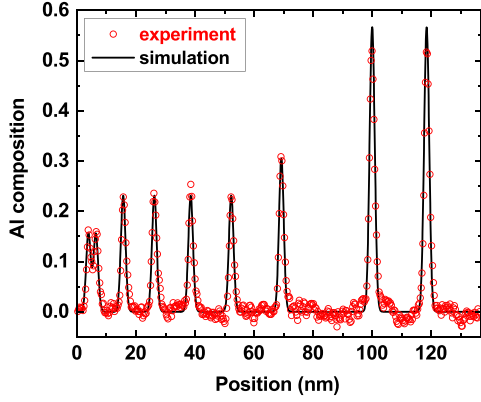


Fig. 5. Al composition (circles) experimentally determined from a g_{002} DFTEM image and the Fourier-transform-based simulated composition profile (line) assuming an interface parameter of 1.6 monolayers [60], [62].

with a zincblende structure [58], [59]. The composition profile with gradual interfaces can easily be simulated in the framework of the Fourier-transform-based model. Fig. 5 shows an experimental composition profile together with the Fourier-transform-based simulated profile for a 4.7-THz QCL [53], [60]. According to [60] and [61], the interface width is about 4.4 times the value of the interface parameter, i.e., 1.6 monolayers. The good agreement between the measured composition profile and the simulated profile allows us to incorporate the actual interface parameters in the simulations of THz QCLs.

D. Fabrication

THz QCLs based on FP resonators and SP waveguides can be straightforwardly fabricated using standard photolithography and wet chemical or dry etching. However, as mentioned above, the active region of THz QCLs based on SP waveguides has to exhibit a comparatively large gain to reach the lasing threshold due to the low confinement factor.

The waveguide and resonator properties affect the operating parameters of the lasers in the following aspects.

- 1) The resonator shape (height, width, and length) influences the thermal properties and, hence, the temperature in the active region since the thermal conductivity through the interfaces in the heterostructure is by about one order of magnitude lower than in bulk GaAs.
- 2) The doping concentration and the thickness of the bottom contact layer as well as the resonator shape determine both the waveguide losses α_{wg} and the confinement factor Γ .
- 3) The parameters of the bottom contact layer also affect how much additional ohmic heat is generated in the system.

For practical reasons, a standard configuration of the bottom contact with a thickness of 700 nm and a Si concentration of $2 \times 10^{18} \text{ cm}^{-3}$ is used for all frequencies. However, there is still room for further improvements since the values for Γ and α_{wg} depend on the thickness and doping concentration of the bottom contact layer as well as on the lasing frequency.

Finally, the geometrical parameters of the laser resonator are relevant for the operating characteristics of the lasers since a

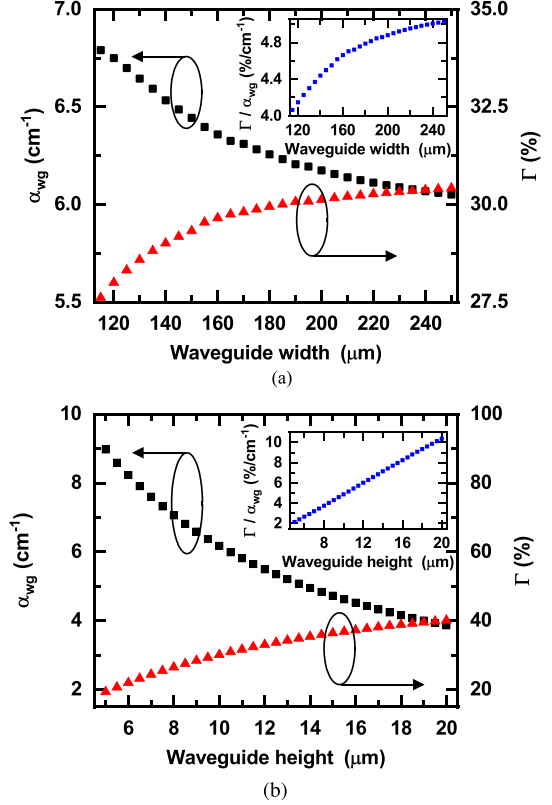


Fig. 6. Simulated values for α_{wg} (squares), Γ (triangles), and Γ/α_{wg} (inset) at 2.6 THz as a function of (a) the waveguide width and (b) height. The simulations were carried out for a trapezoidal cross section and a bottom layer with a thickness of 800 nm and a doping concentration of $9 \times 10^{17} \text{ cm}^{-3}$.

tradeoff between the size and the volume, i.e., the ratio of width and height of the ridge, has to be optimized so that a sufficiently large value for Γ is achieved while minimizing the volume and optical losses. As an example, Fig. 6(a) shows the simulated values for α_{wg} and Γ at 2.6 THz for a 10- μm high SP waveguide as a function of the waveguide width. The inset displays the function Γ/α_{wg} , which increases for wider waveguides without presenting a clear maximum. However, the curve clearly starts to saturate before 200 μm . Fig. 6(b) shows the simulated values as a function of the waveguide height. Both the variations of the waveguide losses and confinement factor are considerably greater than in the previous case. In the simulated height range, Γ/α_{wg} as a function of height displays a remarkably linear behavior [inset of Fig. 6(b)].

However, a thicker active region results in poorer thermal performance as shown for MM waveguides [63]. For SP waveguides, in particular at lower frequencies, further investigation and a redesign of the resonator geometry are still required.

E. THz QCLs for Applications

For practical applications, the THz QCLs have to fulfill a set of specifications for target frequency, tuning range, output power, maximum pumping power, and operability in a Stirling cooler [28], [64]. A typically required output power is about 1 mW. In some cases, also stability during current ramping for

fast frequency tuning may be required [65], [66]. The starting point of the development is the design of an active region that exhibits the gain maximum with a sufficient value at the target frequency. If available, a previous design for a frequency close to the target may be scaled so that the target frequency is reached [12]. Based on this design, the respective wafer is grown and a number of lasers are fabricated and investigated. Since our phenomenological model allows only for a semiquantitative prediction of the lasing parameters, the design parameters have to be adjusted according to the difference between the lasing properties obtained from the simulation and from the experiments. This cycle is repeated until a wafer is obtained, which fulfills the required specifications. Due to the spatial inhomogeneity of the material fluxes in the MBE chamber, the frequency of the gain maximum is a function of the distance from the center of the wafer. Therefore, an appropriate position on the wafer has to be defined [67]. The next step is the preparation of a QCL emitting at the target frequency with a precision of a few GHz, which is determined by the optical length of the resonator with a precision in the micrometer range. If necessary, a post-processing adjustment of the resonator length by facet polishing is performed [68]. For single-mode operation, lateral gratings or two-section resonators may be employed [27]. However, in most cases, when the gain of the active region is sufficiently large, short FP resonators are used.

For high-resolution spectroscopy, a certain frequency tuning is necessary. A typical tuning range of THz QCLs based on the hybrid design and SP waveguides with FP resonators of about 5 GHz is already obtained by intrinsic current tuning, which results from changes of the gain spectrum, and hence the effective refractive index, of the active region with increasing current density [69]. Furthermore, increasing the operating temperature from about 30 to 70 K may also allow for a tuning of the laser modes. For larger tuning ranges, many approaches, such as external optical cavities with continuous tuning ranges of 9–50 GHz [70], [71], microoptomechanical cavities with 240 GHz [72], and electronic frequency tuning in multiterminal and multisection QCLs with 19 GHz [73], have been reported. A technically rather straightforward method is the illumination of the back facet with near-infrared light. Under optimized conditions, a tuning range of up to 40 GHz was reported [74].

III. TABLE-TOP SYSTEMS

THz QCLs as table-top systems are applied in cases that require high-power, high-brilliance, cw radiation. A THz QCL operated in a Stirling cooler (K535, Ricor) was first demonstrated in 2010 by Richter et al. [75]. The typical cooling power of this Stirling cooler is 2.5 W at 40 K and 7 W at 65 K, and has a volume of about $430 \times 280 \times 160 \text{ mm}^3$ as well as a mass of 9.5 kg. An alternative cryocooler is a miniature Stirling cooler (SL400, AIM). The typical cooling power of this cooler is 1.2 W at 40 K and 4 W at 80 K. It has a volume of about $300 \times 120 \times 140 \text{ mm}^3$ as well as a mass of 3.9 kg. Similar systems, such as the TeraCascade 2000 series by Lytid SAS and EasyQCL-100 by LongWave Photonics LLC, are nowadays commercially available.

With the high output power of THz QCLs, real-time high-resolution imaging using THz cameras becomes possible. These cameras are usually based on microbolometer focal-plane array technology derived from the mid-infrared spectral range. The high number of pixels (often over 60 000) requires very high THz powers to illuminate the focal-plane array to maintain high signal-to-noise ratio. The cameras are also more sensitive at higher THz frequencies. As a consequence, THz QCLs are an ideal match to these cameras for imaging applications. As an example, phase retrieval phase imaging using a table-top THz QCL system was demonstrated [76]. Furthermore, the high long-term power stability of THz QCLs integrated in table-top systems with cryogen-free cryocoolers has allowed for the development of extremely sensitive sensors for bio-sensing based on probing liquids in the THz range [77]. Uncooled microbolometer cameras are commercially available, such as the uncooled focal-plane array microbolometer camera in highly versatile THz imaging system (TeraEyes-HV) by Lytid SAS and uncooled focal-plane array microbolometer array in uncooled real-time THz imager by Swiss THz.

Recently, cw THz radiation sources at frequencies below 2.5 THz have increasingly demanded for applications, such as nondestructive testing on industrial composite parts [78]. For this application, low-frequency sources could maximize transmission, i.e., penetration depths beyond 1–2 mm, through the sample made of polypropylene plastic with still excellent resolution. As commercial cw THz sources in the range of 1–2 THz with sufficient power ($>1 \text{ mW}$) are still not available, extending THz QCLs to the low-frequency range below 2.5 THz is required.

For emission frequencies between 1.6 and 2.0 THz, several QCLs based on BTC designs and GaAs/Al_{0.1}Ga_{0.9}As heterostructures have been reported [79], [80], [81]. For this frequency range, neither the hybrid design nor the GaAs/AlAs materials system has been shown to be the best choice so far. In the hybrid design, the photon energy is very small compared with the LO phonon energy, which leads to a rather low wall plug efficiency. On the contrary, the operating field strength for this design type decreases with decreasing emission frequency. Therefore, the limits of the hybrid design are still not yet fully explored. Furthermore, the laser levels are very close to the conduction band edge, which results in rather high effective barriers and correspondingly low coupling through the barriers. To maintain resonant tunneling in this case, the barriers would have to be extremely thin. Recently, we developed a 2.6-THz QCL based on a hybrid design using a GaAs/Al_{0.18}Ga_{0.82}As heterostructure (QCL A).¹ In comparison with the BTC-design-based QCL operating below 2 THz, the current density of QCL A is large, but it can be operated in a single mode. The QCLs below 2.5 THz would be approached by a scaling of the layer structure of 2.6 THz QCLs as well as slight adjustments of the thicknesses of the main quantum wells and some barriers.

¹QCL A corresponds to sample PDI-M4-3991. The nominal layer sequence starting from the injection barrier is **4.0**, 35.6, **2.0**, 17.6, **2.4**, 13.9, **2.2**, 11.2, **2.2**, 9.5, **2.2**, 8.7, **2.2**, 7.7, **2.7**, 19.2, **3.0**, and 19.8 with the layer thicknesses in nm. Bold numbers denote the Al_{0.18}Ga_{0.82}As barriers, whereas the underlined number indicates the doped layer. The nominal doping density is $0.7 \times 10^{17} \text{ cm}^{-3}$.

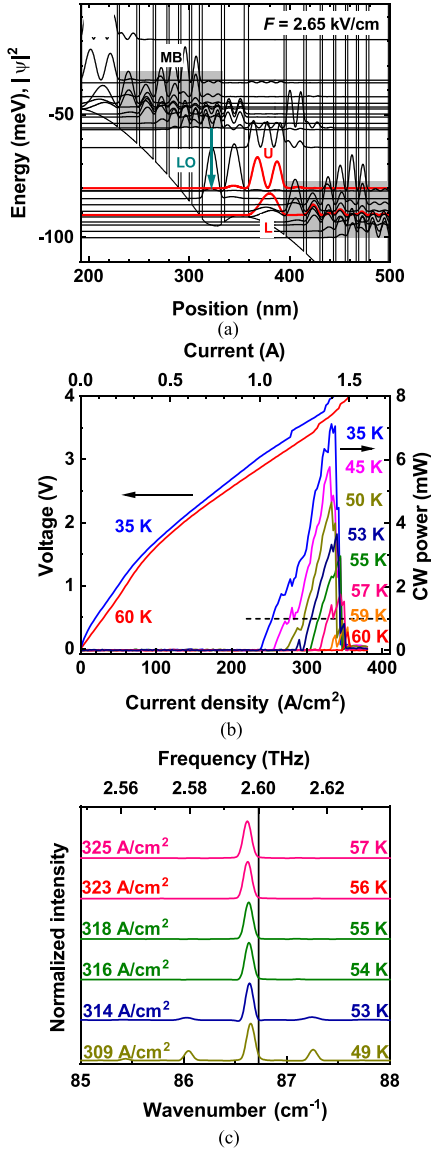


Fig. 7. (a) Conduction band profile as well as subband structure, (b) L - J - V characteristics for several operating temperatures, and (c) lasing spectra for several operating temperatures and current densities of QCL A under cw operation with laser ridge dimensions of $0.20 \times 2.105 \text{ mm}^2$. The dashed line in (a) indicates the power of 1 mW and the vertical line in (b) indicates the frequency of 2.6 THz as a guide to the eye.

The output power of all THz QCLs was determined using a power meter (SLT THz 20) in front of the vacuum window of the cryocooler, which was calibrated by the German National Metrology Institute (Physikalisch-Technische Bundesanstalt). We do not correct the measured output power for factors, such as collection efficiency, water absorption, or two-facet emission, so that the values are always the lower bound for the actual power.

Fig. 7 shows the subband structure and the L - J - V characteristics as well as the lasing spectra of QCL A under various operating conditions. The wall plug efficiency for QCL A reaches a value of 1.1×10^{-3} . The active region needs still to be optimized to improve the wall plug efficiency. For a temperature up to 57 K, the QCL emits always in a single mode with an output power larger than 1 mW. For a laser, which is processed from a similar

position of the wafer but mounted in a TeraCascade 2000 system and operated at 46 K, the maximum cw output power reaches about 3 mW.

Table-top systems are also used for local oscillators in heterodyne spectrometers and for absorption spectrometers. From 2014 to 2022, local oscillators based on the 4.7-THz QCLs have been used in the German Receiver for Astronomy at Terahertz Frequencies (GREAT) and upGREAT on board the Stratospheric Observatory for Infrared Astronomy for the detection of atomic oxygen [64], [82], [83]. In 2022, a 4.7-THz QCL local oscillator has been employed in an oxygen spectrometer for atmospheric science on a balloon (OSAS-B) for the study of atomic oxygen in the mesosphere and lower thermosphere of the Earth [84], [85]. THz QCLs have also been applied as radiation source in an absorption spectrometer for the determination of the atomic oxygen densities in plasmas [65], [66].

IV. THz QCLs FOR HETERODYNE SPECTROSCOPY

High-resolution heterodyne spectroscopy is the method of choice for observing narrow-band molecular and atomic transitions in the THz range in astronomy and atmospheric research. Atomic oxygen, as an example, is very important for the energy balance of the mesosphere and lower thermosphere of Earth, where it is the dominant species [83], [86]. It is also found in the atmosphere of other planets, such as Mars and Venus [82], [87]. The $^3P_1 \rightarrow ^3P_2$ fine-structure transition of neutral atomic oxygen (OI) emits and absorbs electromagnetic radiation with a rest frequency of 4.744777 THz [83], [88].

Another species is the hydroxyl radical (OH), which plays a significant role in the chemistry of the Earth's atmosphere and the interstellar media. The $^1F_{5/2} \rightarrow ^1F_{7/2}$ rotational transition of OH with an emission frequency of 3.551192 THz [89] is also accessible by heterodyne detection. Heterodyne spectroscopy relies on the mixing of the radiation to be detected with the radiation from a so-called local oscillator, which is detuned somewhat, so that the difference frequency between them is measured. If the frequency of the local oscillator is precisely known, the frequency of the detected signal can be determined. The effective linewidth of the QCL has to be as small as possible. To achieve effective linewidths below 1 MHz, the QCL is passively or even actively stabilized. The passive stabilization is based on thermal and electrical bias control [64], whereas the active stabilization is based on frequency reference, such as a molecular transition frequency [90].

Fig. 8 shows the L - J - V characteristics and emission spectra of a recently optimized high-performance, 3.5-THz QCL (QCL B),² which has been shown in Fig. 4 and exhibits an output power of 10 mW, under various operating conditions. The wall plug efficiency for QCL B approaches about 4.8×10^{-3} . The target frequency of 3.55 THz can be reached by selecting an appropriate location on the wafer for the laser by using the

²QCL B corresponds to sample PDI-M3-2357. The nominal layer sequence starting from the injection barrier is **0.84**, 32.2, **0.48**, 16.9, **0.48**, 13.1, **0.48**, 11.7, **0.48**, 10.5, **0.48**, 9.6, **0.48**, 20.0, **0.84**, and 19.1 with the layer thicknesses in nm. Bold numbers denote the AlAs barriers, whereas the underlined number indicates the doped layer. The nominal doping density is $2.0 \times 10^{17} \text{ cm}^{-3}$.

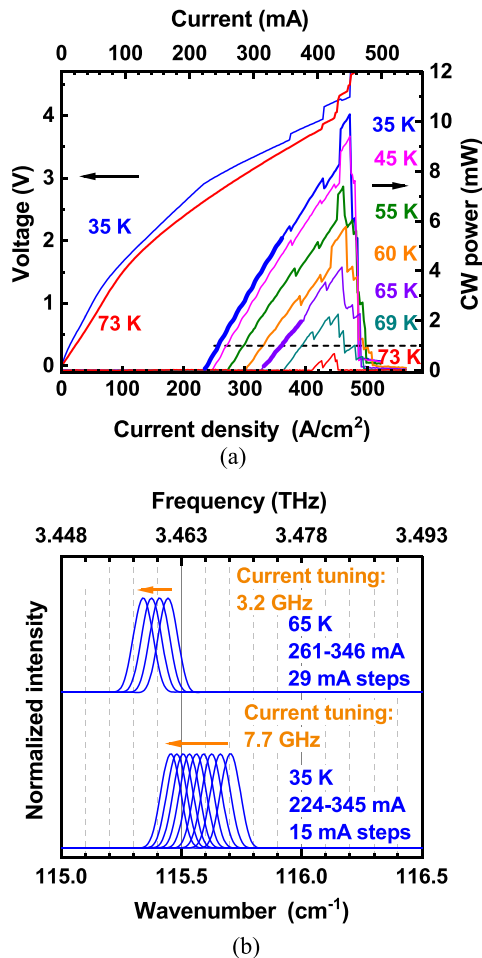


Fig. 8. (a) L - J - V characteristics for several operating temperatures and (b) lasing spectra for two operating temperatures and several current densities of QCL B under cw operation with laser ridge dimensions of $0.12 \times 0.795 \text{ mm}^2$. The thick solid lines of the L - J curves in (a) show the range of the current corresponding to the spectra in (b). The dashed line in (a) indicates the power of 1 mW as a guide to the eye.

correlation between frequency and location [67]. At 35 K and in the current range between 224 and 345 mA, the electrical pump power of QCL B is below the cooling power of the Stirling cryocooler (Ricor K535) of about 1.2 W so that the laser can be stably operated. Under these conditions, the current tuning range is 7.7 GHz at output powers up to 5.3 mW. At a heat sink temperature of 65 K, QCL B exhibits always single-mode emission, as shown in Fig. 8(b). The tuning properties are important for the frequency calibration of the QCL local oscillator.

For heterodyne spectroscopy of particular molecular and atomic transitions, the emission frequency characteristic of the QCL has to be known with high precision. The calibration can be done with the help of the spectral finger print of a well-known molecule, such as methanol [28]. For the laser shown in Fig. 8, we measured the power signal transmitted through an absorption cell, which is filled with methanol at a pressure of 100 Pa. Fig. 9(a) displays the transmitted power as a function of applied current and heat sink temperature for QCL B in the range of 200–500 mA and above 12 K. The used cryocooler (Sumitomo, SRDK-408D) has a cooling capacity of

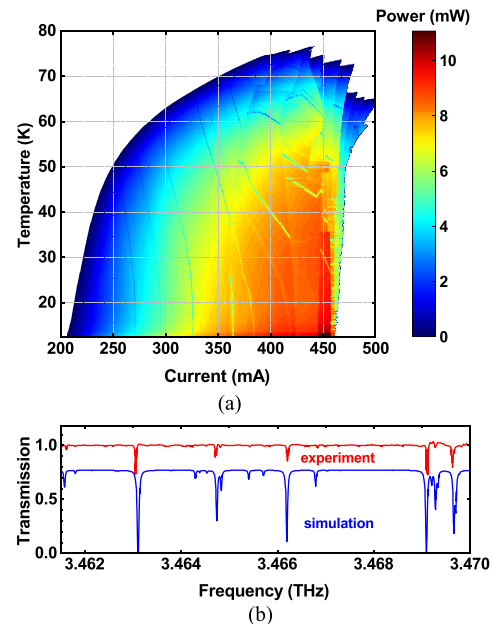


Fig. 9. (a) Optical output power as a function of applied current and heat sink temperature of QCL B. The measurement shows a series of lines due to the absorption by the methanol gas. (b) Measured absorption spectrum (red line) as well as the result of a simulation (blue line, offset: -0.22) for line identification in the cryocooler at 20 K, with a tuning coefficient of -60 MHz/mA .

about 1 W at 4.2 K. Fig. 9(b) shows the absorption spectrum between 200 and 360 mA at 20 K corresponding to Fig. 9(a). For frequency calibration, the measured absorption spectrum (red line) is compared with a calculated transmission spectrum (blue line) based on the Jet Propulsion Laboratory database [91], which eventually yields the frequency axis.

A recent instrument with a QCL local oscillator is the OSAS-B. OSAS-B is a heterodyne receiver for observing the 4.75-THz emission from atomic oxygen in the mesosphere and lower thermosphere [84], [85]. The spectrometer frontend is composed of a superconducting hot-electron bolometer as the mixer and a 4.75-THz GaAs/AlAs QCL³ as the local oscillator. In this system, the QCL has been operated in a liquid/solid nitrogen stage for cooling. Since the OI line is obscured by water absorption in the troposphere, observations take place from the gondola of a stratospheric balloon. Fig. 10 depicts examples for the OI emission signal for two observation angles (elevation) using the 4.75-THz QCL described in [28]. The sub-MHz linewidth of the local-oscillator QCL enables the resolution of subtle spectral features in the line shape of OI. These are in particular present at low elevation angles, and reflect the interplay of contributions from different altitudes.

³QCL for OSAS-B corresponds to sample PDI-M4-3011. The nominal layer sequence starting from the injection barrier is **1.12**, 27.2, **0.56**, 15.0, **0.42**, 12.1, **0.42**, 10.8, **0.42**, 9.2, **0.42**, 8.1, **0.28**, 2.0, **0.28**, 17.7, **1.12**, and 15.7 with the layer thicknesses in nm. Bold numbers denote the AlAs barriers, whereas the underlined number indicates the doped layer. The nominal doping density is $2.0 \times 10^{17} \text{ cm}^{-3}$.

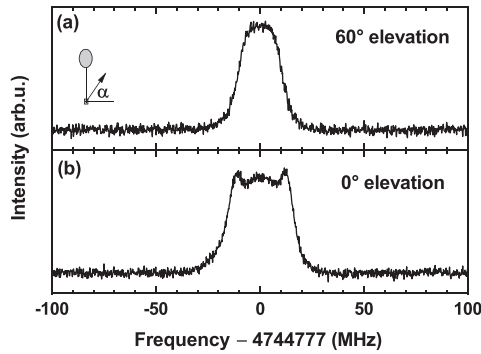


Fig. 10. 4.75-THz emission of OI as measured with the OSAS-B heterodyne receiver at (a) 60° elevation and (b) 0° elevation. The wing structure in the spectrum at low elevation is due to an interplay of absorption and emission from layers of the atmosphere with large temperature differences.

V. THz QCLS FOR ABSORPTION SPECTROSCOPY

In plasma science and technology, the dynamics of atomic and ionic species play a significant role in the plasma chemistry. The detection of these species as well as an accurate determination of their densities is of key importance for understanding the chemical behavior of plasmas and optimizing industrial processes. Absorption spectroscopy in the THz range enables the detection of process-relevant species by using transitions between fine structure levels of ground-state atoms and ions, which typically lie in the THz spectral region. For example, Al atoms, N^+ ions, and O atoms exhibit fine structure transitions at 3.360, 3.921, and 4.745 THz, respectively.

Although the same fine structure transition of atomic oxygen as in astronomy and atmospheric research is used, the measurement principle is now based on absorption rather than emission. Generally, to obtain information on the density of absorbing species in a plasma, laser radiation with a specific frequency is sent through the plasma and the transmitted radiation is detected. By tuning the frequency of the laser across an absorption line, the lineshape of the absorption feature can be recorded. If the laser linewidth is sufficiently narrow, the lineshape of the absorption feature is mainly determined by Doppler broadening (for low-pressure plasmas), therefore providing the temperature of the investigated species. This is a crucial parameter needed to derive absolute ground-state densities from the measured absorption spectra. So, a tuning range that covers the complete absorption feature of interest is an important requirement for QCLs to be used as radiation source for THz absorption spectroscopy. For real-time measurements, a fast tuning of the emission frequency of the QCL and, hence, a fast ramping of the driving current are required. During the fast ramping, no instabilities are allowed, which is an additional requirement for the specifications of the QCL.

Fig. 11 shows the L - J - V characteristics of QCL C⁴ for the detection of O atoms (transition at 4.7448 THz) under various operating conditions [65]. This laser shows no instabilities during fast ramping of the current. However, the current density is

⁴QCL C corresponds to sample PDI-M4-3146. The nominal layer sequence is the same as the QCL for OSAS-B. The nominal doping density is $3.0 \times 10^{17} \text{ cm}^{-3}$.

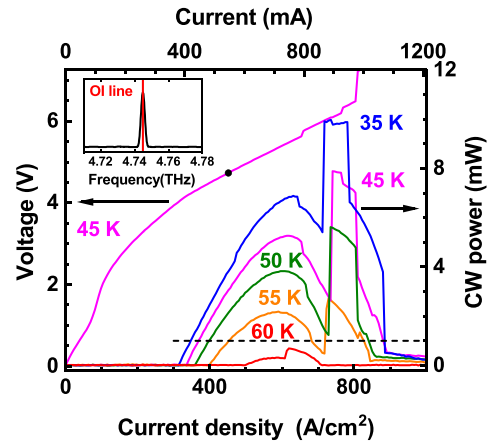


Fig. 11. L - J - V characteristics for several operating temperatures of QCL C under cw operation with laser ridge dimensions of $0.12 \times 1.01 \text{ mm}^2$. The dashed line indicates the power of 1 mW as a guide to the eye. Inset: QCL emission spectrum. At the driving current-temperature setting $J = 451 \text{ A/cm}^2$ (547 mA) and 45 K, the QCL emits a single mode at 4.7448 THz.

relatively large so that it can be operated only over a part of the dynamic range. Nevertheless, at 45 K, the current tuning range approaches 3.7 GHz, and the maximum output power reaches 3.4 mW in the reduced dynamic range for stable operation. For the large frequency range, the laser emits light with only one frequency, i.e., in a single mode. As an example, the emission spectrum is shown in the inset of Fig. 11, which is measured at a current density of 451 A/cm^2 (547 mA), corresponding to the dot in Fig. 11. In the temperature range between 45 and 55 K, this QCL emits a single mode and the overall tuning range is 10 GHz.

QCL C has been demonstrated to be suitable for accurate measurements of atomic oxygen densities in plasmas. Using the experimental setup described in [66] and [92], the fine structure transition of atomic oxygen was successfully detected in a capacitively coupled radio-frequency (CCRF) oxygen plasma. The measured absorption spectral profiles were analyzed to obtain the atomic oxygen density and temperature. By changing the pressure (0.7–1.3 mbar) and RF power (20–100 W), the influence of external parameters on the density of atomic oxygen was investigated.

In previous works [66], [92], laser tuning frequencies of 10 or 11 Hz were used (corresponding to a current ramp of 0.2 A/s or less). Faster measurements were hampered by the limited bandwidth of the used bolometer, leading to an asymmetric deformation of the observed absorption features [66]. A recently developed THz detector (Laser Components Germany GmbH, PR No1) with a significantly larger bandwidth allows for faster measurements, with laser tuning frequencies up to 1 kHz (corresponding to approximately 26 A/s) without deforming the absorption features [93]. For these frequencies, the laser showed stable behavior, i.e., the maximum current ramping speed is still limited by the detector rather than the laser characteristics.

In addition to the ammonia gas measurements presented in [93], we used the pyroelectric THz detector for measuring

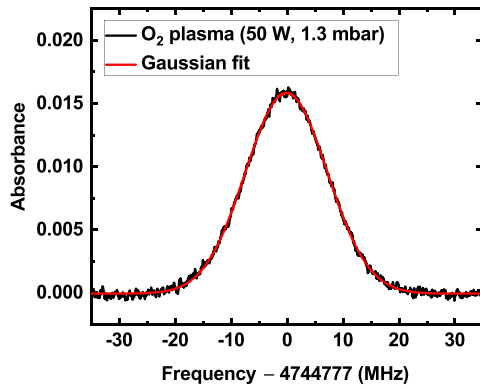


Fig. 12. Spectral absorption profile of the fine structure transition of atomic oxygen at 4.7448 THz, measured in an oxygen plasma (applied RF power of 50 W and gas pressure of 1.3 mbar). QCL C was operated at 44.30 K with a tuning frequency of 201 Hz and a current ramp of approximately 1.4 A/s.

atomic oxygen densities in the CCRF oxygen plasma by applying fast ramping. A typical example of the spectral profile of the atomic oxygen transition obtained with a laser tuning frequency of 201 Hz and a current ramp of approximately 1.4 A/s is shown in Fig. 12.

In [92], THz absorption spectroscopy was benchmarked against a more established yet complex and expensive method, namely, two-photon absorption laser induced fluorescence. The results are in good agreement and demonstrate that QCL-based THz absorption spectroscopy is an accurate technique that can be reliably used for real-world applications, most noteworthy the microelectronics industry, to measure atomic oxygen densities in plasmas.

VI. CONCLUSION

We have developed THz QCLs based on GaAs/Al_xGa_{1-x}As heterostructures for frequencies between 2.6 and 4.7 THz using SP waveguides. In particular, GaAs/AlAs QCLs exhibit cw output powers of up to 10 mW. These lasers are operated in mechanical cryocoolers, which is beneficial for practical applications. Single-mode operation with sufficient tuning range is realized using short FP cavities. THz QCLs are employed for high-resolution heterodyne and absorption spectroscopy in astronomy and plasma diagnostics, respectively. Furthermore, THz QCLs are integrated into table-top commercial THz sources, which are important instruments for current research and development in the field of THz science and technology. Meanwhile, THz QCLs have been proven to be powerful radiation sources for a number of practical applications.

ACKNOWLEDGMENT

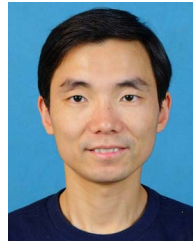
The authors would like to thank H. T. Grahn for his very valuable contribution to the development of the QCLs, W. Anders, N. Volkmer, C. Herrmann, D. Steffen, A. Riedel, and A. Tahraoui for sample preparation, and T. Flissikowski for a careful reading of this article.

REFERENCES

- [1] J. Faist et al., "Quantum cascade laser," *Science*, vol. 264, pp. 553–556, Apr. 1994, doi: [10.1126/science.264.5158.553](https://doi.org/10.1126/science.264.5158.553).
- [2] R. Köhler et al., "Terahertz semiconductor-heterostructure laser," *Nature*, vol. 417, pp. 156–159, May 2002, doi: [10.1038/417156a](https://doi.org/10.1038/417156a).
- [3] M. Rochat et al., "Low-threshold terahertz quantum-cascade lasers," *Appl. Phys. Lett.*, vol. 81, no. 8, pp. 1381–1383, Aug. 2002, doi: [10.1063/1.1498861](https://doi.org/10.1063/1.1498861).
- [4] B. S. Williams, H. Callebaut, S. Kumar, Q. Hu, and J. L. Reno, "3.4-THz quantum cascade laser based on longitudinal-optical-phonon scattering for depopulation," *Appl. Phys. Lett.*, vol. 82, no. 7, pp. 1015–1017, Feb. 2003, doi: [10.1063/1.1554479](https://doi.org/10.1063/1.1554479).
- [5] S. Kumar, C. W. I. Chan, Q. Hu, and J. L. Reno, "Two-well terahertz quantum-cascade laser with direct intrawell-phonon depopulation," *Appl. Phys. Lett.*, vol. 95, no. 14, Oct. 2009, Art. no. 141110, doi: [10.1063/1.3243459](https://doi.org/10.1063/1.3243459).
- [6] G. Scalari et al., "Far-infrared ($\lambda \simeq 87 \mu\text{m}$) bound-to-continuum quantum-cascade lasers operating up to 90 K," *Appl. Phys. Lett.*, vol. 82, no. 19, pp. 3165–3167, May 2003, doi: [10.1063/1.1571653](https://doi.org/10.1063/1.1571653).
- [7] A. Khalatpour, A. K. Paulsen, C. Deimert, Z. R. Wasilewski, and Q. Hu, "High-power portable terahertz laser systems," *Nature Photon.*, vol. 15, pp. 16–20, Jan. 2021, doi: [10.1038/s41566-020-00707-5](https://doi.org/10.1038/s41566-020-00707-5).
- [8] A. Khalatpour et al., "Enhanced operating temperature in terahertz quantum cascade lasers based on direct phonon depopulation," *Appl. Phys. Lett.*, vol. 122, no. 16, Apr. 2023, Art. no. 161101, doi: [10.1063/5.0144705](https://doi.org/10.1063/5.0144705).
- [9] R. Köhler et al., "Terahertz quantum-cascade lasers based on an interlaced photon-phonon cascade," *Appl. Phys. Lett.*, vol. 84, no. 8, pp. 1266–1268, Feb. 2004, doi: [10.1063/1.1650905](https://doi.org/10.1063/1.1650905).
- [10] G. Scalari, N. Hoyler, M. Giovannini, and J. Faist, "Terahertz bound-to-continuum quantum-cascade lasers based on optical-phonon scattering extraction," *Appl. Phys. Lett.*, vol. 86, no. 18, Apr. 2005, Art. no. 181101, doi: [10.1063/1.1920407](https://doi.org/10.1063/1.1920407).
- [11] M. Wienold et al., "Low-voltage terahertz quantum-cascade lasers based on LO-phonon-assisted interminiband transitions," *Electron. Lett.*, vol. 45, no. 20, pp. 1030–1031, Sep. 2009, doi: [10.1049/el.2009.1371](https://doi.org/10.1049/el.2009.1371).
- [12] L. Schrottke et al., "High-performance GaAs/AlAs terahertz quantum-cascade lasers for spectroscopic applications," *IEEE Trans. THz Sci. Technol.*, vol. 10, no. 2, pp. 133–140, Mar. 2020, doi: [10.1109/TTHZ.2019.2957456](https://doi.org/10.1109/TTHZ.2019.2957456).
- [13] L. Schrottke, M. Giehler, M. Wienold, R. Hey, and H. T. Grahn, "Compact model for the efficient simulation of the optical gain and transport properties in THz quantum-cascade lasers," *Semicond. Sci. Technol.*, vol. 25, no. 4, Apr. 2010, Art. no. 045025, doi: [10.1088/0268-1242/25/4/045025](https://doi.org/10.1088/0268-1242/25/4/045025).
- [14] L. Schrottke, X. Lü, and H. T. Grahn, "Fourier transform-based scattering-rate method for self-consistent simulations of carrier transport in semiconductor heterostructures," *J. Appl. Phys.*, vol. 117, no. 15, Apr. 2015, Art. no. 154309, doi: [10.1063/1.4918671](https://doi.org/10.1063/1.4918671).
- [15] X. Lü, L. Schrottke, and H. T. Grahn, "Fourier-transform-based model for carrier transport in semiconductor heterostructures: Longitudinal optical phonon scattering," *J. Appl. Phys.*, vol. 119, no. 21, Jun. 2016, Art. no. 214302, doi: [10.1063/1.4952741](https://doi.org/10.1063/1.4952741).
- [16] C. Deutsch et al., "Terahertz quantum cascade lasers based on type II InGaAs/GaAsSb/InP," *Appl. Phys. Lett.*, vol. 97, no. 26, Dec. 2010, Art. no. 261110, doi: [10.1063/1.3532106](https://doi.org/10.1063/1.3532106).
- [17] M. Brandstetter et al., "InAs based terahertz quantum cascade lasers," *Appl. Phys. Lett.*, vol. 108, no. 1, Jan. 2016, Art. no. 011109, doi: [10.1063/1.4939551](https://doi.org/10.1063/1.4939551).
- [18] J. L. Kloosterman et al., "Hot electron bolometer heterodyne receiver with a 4.7-THz quantum cascade laser as a local oscillator," *Appl. Phys. Lett.*, vol. 102, no. 1, Jan. 2013, Art. no. 011123, doi: [10.1063/1.4774085](https://doi.org/10.1063/1.4774085).
- [19] M. Wienold et al., "High-temperature, continuous-wave operation of terahertz quantum-cascade lasers with metal-metal waveguides and third-order distributed feedback," *Opt. Exp.*, vol. 22, no. 3, pp. 3334–3348, Feb. 2014, doi: [10.1364/OE.22.003334](https://doi.org/10.1364/OE.22.003334).
- [20] L. Bosco et al., "A patch-array antenna single-mode low electrical dissipation continuous wave terahertz quantum cascade laser," *Appl. Phys. Lett.*, vol. 109, no. 20, Nov. 2016, Art. no. 201103, doi: [10.1063/1.4967836](https://doi.org/10.1063/1.4967836).
- [21] A. Khalatpour et al., "A tunable unidirectional source for GUSTO's local oscillator at 4.74 THz," *IEEE Trans. THz Sci. Technol.*, vol. 12, no. 2, pp. 144–150, Mar. 2022, doi: [10.1109/tthz.2021.3124310](https://doi.org/10.1109/tthz.2021.3124310).
- [22] B. S. Williams, "Terahertz quantum-cascade lasers," *Nature Photon.*, vol. 1, pp. 517–525, Sep. 2007, doi: [10.1038/nphoton.2007.166](https://doi.org/10.1038/nphoton.2007.166).

- [23] B. S. Williams, S. Kumar, Q. Hu, and J. L. Reno, "Distributed-feedback terahertz quantum-cascade lasers with laterally corrugated metal waveguides," *Opt. Lett.*, vol. 30, no. 21, pp. 2909–2911, Nov. 2005, doi: [10.1364/ol.30.002909](https://doi.org/10.1364/ol.30.002909).
- [24] L. Mahler et al., "High-performance operation of single-mode terahertz quantum cascade lasers with metallic gratings," *Appl. Phys. Lett.*, vol. 87, no. 18, Oct. 2005, Art. no. 181101, doi: [10.1063/1.2120901](https://doi.org/10.1063/1.2120901).
- [25] M. Wienold et al., "Lateral distributed-feedback gratings for single-mode, high-power terahertz quantum-cascade lasers," *Opt. Exp.*, vol. 20, no. 10, pp. 11207–11217, 2012, doi: [10.1364/OE.20.011207](https://doi.org/10.1364/OE.20.011207).
- [26] H. Li et al., "Coupled-cavity terahertz quantum cascade lasers for single mode operation," *Appl. Phys. Lett.*, vol. 104, no. 24, Jun. 2014, Art. no. 241102, doi: [10.1063/1.4884056](https://doi.org/10.1063/1.4884056).
- [27] M. Hempel et al., "Continuous tuning of two-section, single-mode terahertz quantum-cascade lasers by fiber-coupled, near-infrared illumination," *AIP Adv.*, vol. 7, no. 5, May 2017, Art. no. 055201, doi: [10.1063/1.4983030](https://doi.org/10.1063/1.4983030).
- [28] T. Hagelschuer et al., "A compact 4.75-THz source based on a quantum-cascade laser with a back-facet mirror," *IEEE Trans. THz Sci. Technol.*, vol. 9, no. 6, pp. 606–612, Nov. 2019, doi: [10.1109/TTHZ.2019.2935337](https://doi.org/10.1109/TTHZ.2019.2935337).
- [29] C. Belacel et al., "Optomechanical terahertz detection with single meta-atom resonator," *Nature Commun.*, vol. 8, no. 1, Nov. 2017, Art. no. 1578, doi: [10.1038/s41467-017-01840-6](https://doi.org/10.1038/s41467-017-01840-6).
- [30] R. Degl'Innocenti et al., "Fast room-temperature detection of terahertz quantum cascade lasers with graphene-loaded bow-tie plasmonic antenna arrays," *ACS Photon.*, vol. 3, no. 10, pp. 1747–1753, Sep. 2016, doi: [10.1021/acsp Photonics.6b00405](https://doi.org/10.1021/acsp Photonics.6b00405).
- [31] B. N. Behnken, G. Karunasiri, D. R. Chamberlin, P. R. Robrish, and J. Faist, "Real-time imaging using a 2.8 THz quantum cascade laser and uncooled infrared microbolometer camera," *Opt. Lett.*, vol. 33, no. 5, pp. 440–442, Feb. 2008, doi: [10.1364/ol.33.000440](https://doi.org/10.1364/ol.33.000440).
- [32] N. Rothbart et al., "Fast 2-D and 3-D terahertz imaging with a quantum-cascade laser and a scanning mirror," *IEEE Trans. THz Sci. Technol.*, vol. 3, no. 5, pp. 617–624, Sep. 2013, doi: [10.1109/tthz.2013.2273226](https://doi.org/10.1109/tthz.2013.2273226).
- [33] P. Dean et al., "Terahertz imaging using quantum cascade lasers—A review of systems and applications," *J. Phys. D: Appl. Phys.*, vol. 47, no. 37, Aug. 2014, Art. no. 374008, doi: [10.1088/0022-3727/47/37/374008](https://doi.org/10.1088/0022-3727/47/37/374008).
- [34] D. Burghoff et al., "Terahertz laser frequency combs," *Nature Photon.*, vol. 8, no. 6, pp. 462–467, Jun. 2014, doi: [10.1038/nphoton.2014.85](https://doi.org/10.1038/nphoton.2014.85).
- [35] M. Rösch, G. Scalari, M. Beck, and J. Faist, "Octave-spanning semiconductor laser," *Nature Photon.*, vol. 9, pp. 42–47, 2015, doi: [10.1038/nphoton.2014.279](https://doi.org/10.1038/nphoton.2014.279).
- [36] N. Picqué and T. W. Hänsch, "Frequency comb spectroscopy," *Nature Photon.*, vol. 13, no. 3, pp. 146–157, Feb. 2019, doi: [10.1038/s41566-018-0347-5](https://doi.org/10.1038/s41566-018-0347-5).
- [37] M. C. Giordano et al., "Phase-resolved terahertz self-detection near-field microscopy," *Opt. Exp.*, vol. 26, no. 14, Jul. 2018, Art. no. 18423, doi: [10.1364/oe.26.018423](https://doi.org/10.1364/oe.26.018423).
- [38] C. Silvestri, L. L. Columbo, and M. Brambilla, "Retrieval of the dielectric properties of a resonant material in the terahertz region via self-detection near field optical microscopy," *IEEE J. Sel. Top. Quantum Electron.*, vol. 29, no. 5: Terahertz Photonics, pp. 1–11, Sep./Oct. 2023, doi: [10.1109/jstqe.2023.3287041](https://doi.org/10.1109/jstqe.2023.3287041).
- [39] H.-W. Hübers, M. F. Kimmitt, N. Hiromoto, and E. Brundermann, "Terahertz spectroscopy: System and sensitivity considerations," *IEEE Trans. THz Sci. Technol.*, vol. 1, no. 1, pp. 321–331, Sep. 2011, doi: [10.1109/tthz.2011.2159877](https://doi.org/10.1109/tthz.2011.2159877).
- [40] C. Jirauschek and T. Kubis, "Modeling techniques for quantum cascade lasers," *Appl. Phys. Rev.*, vol. 1, 2014, Art. no. 011307, doi: [10.1063/1.4863665](https://doi.org/10.1063/1.4863665).
- [41] K. Donovan, P. Harrison, and R. W. Kelsall, "Self-consistent solutions to the intersubband rate equations in quantum cascade lasers: Analysis of a GaAs/Al_xGa_{1-x}As device," *J. Appl. Phys.*, vol. 89, no. 6, pp. 3084–3090, Jun. 2001, doi: [10.1063/1.1341216](https://doi.org/10.1063/1.1341216).
- [42] D. Indjin, P. Harrison, R. W. Kelsall, and Z. Ikonjić, "Self-consistent scattering theory of transport and output characteristics of quantum cascade lasers," *J. Appl. Phys.*, vol. 91, no. 11, pp. 9019–9026, Jun. 2002, doi: [10.1063/1.1474613](https://doi.org/10.1063/1.1474613).
- [43] R. C. Iotti and F. Rossi, "Nature of charge transport in quantum-cascade lasers," *Phys. Rev. Lett.*, vol. 87, Sep. 2001, Art. no. 146603, doi: [10.1103/PhysRevLett.87.146603](https://doi.org/10.1103/PhysRevLett.87.146603).
- [44] C. Jirauschek, A. Matyas, and P. Lugli, "Modeling bound-to-continuum terahertz quantum cascade lasers: The role of Coulomb interactions," *J. Appl. Phys.*, vol. 107, no. 1, Jan. 2010, Art. no. 013104, doi: [10.1063/1.3276160](https://doi.org/10.1063/1.3276160).
- [45] A. Wacker, "Gain in quantum cascade lasers and superlattices: A quantum transport theory," *Phys. Rev. B*, vol. 66, Aug. 2002, Art. no. 085326, doi: [10.1103/PhysRevB.66.085326](https://doi.org/10.1103/PhysRevB.66.085326).
- [46] S.-C. Lee and A. Wacker, "Nonequilibrium Green's function theory for transport and gain properties of quantum cascade structures," *Phys. Rev. B*, vol. 66, Art. no. 245314, Dec. 2002, doi: [10.1103/PhysRevB.66.245314](https://doi.org/10.1103/PhysRevB.66.245314).
- [47] A. Wacker, M. Lindskog, and D. O. Winge, "Nonequilibrium Green's function model for simulation of quantum cascade laser devices under operating conditions," *IEEE J. Sel. Top. Quantum Electron.*, vol. 19, no. 5, Sep./Oct. 2013, Art. no. 1200611, doi: [10.1109/JSTQE.2013.2239613](https://doi.org/10.1109/JSTQE.2013.2239613).
- [48] T. Kubis et al., "Theory of nonequilibrium quantum transport and energy dissipation in terahertz quantum cascade lasers," *Phys. Rev. B*, vol. 79, 2009, Art. no. 195323, doi: [10.1103/PhysRevB.79.195323](https://doi.org/10.1103/PhysRevB.79.195323).
- [49] S. Kumar and Q. Hu, "Coherence of resonant-tunneling transport in terahertz quantum-cascade lasers," *Phys. Rev. B*, vol. 80, Dec. 2009, Art. no. 245316, doi: [10.1103/PhysRevB.80.245316](https://doi.org/10.1103/PhysRevB.80.245316).
- [50] E. Dupont, S. Fatholouloumi, and H. C. Liu, "Simplified density-matrix model applied to three-well terahertz quantum cascade lasers," *Phys. Rev. B*, vol. 81, 2010, Art. no. 205311, doi: [10.1103/PhysRevB.81.205311](https://doi.org/10.1103/PhysRevB.81.205311).
- [51] G. Beji, Z. Ikonjić, C. A. Evans, D. Indjin, and P. Harrison, "Coherent transport description of the dual-wavelength ambipolar terahertz quantum cascade laser," *J. Appl. Phys.*, vol. 109, 2011, Art. no. 013111, doi: [10.1063/1.3530628](https://doi.org/10.1063/1.3530628).
- [52] A. Pan, B. A. Burnett, C. O. Chui, and B. S. Williams, "Density matrix modeling of quantum cascade lasers without an artificially localized basis: A generalized scattering approach," *Phys. Rev. B*, vol. 96, no. 8, Aug. 2017, Art. no. 085308, doi: [10.1103/physrevb.96.085308](https://doi.org/10.1103/physrevb.96.085308).
- [53] X. Lü, L. Schrottke, E. Luna, and H. T. Grahn, "Efficient simulation of the impact of interface grading on the transport and optical properties of semiconductor heterostructures," *Appl. Phys. Lett.*, vol. 104, no. 23, Jun. 2014, Art. no. 232106, doi: [10.1063/1.4882653](https://doi.org/10.1063/1.4882653).
- [54] L. Schrottke, X. Lü, G. Rozas, K. Biermann, and H. T. Grahn, "Terahertz GaAs/AlAs quantum-cascade lasers," *Appl. Phys. Lett.*, vol. 108, no. 10, Mar. 2016, Art. no. 102102, doi: [10.1063/1.4943657](https://doi.org/10.1063/1.4943657).
- [55] K. Biermann et al., "In-situ control of molecular beam epitaxial growth by spectral reflectivity analysis," *J. Cryst. Growth*, vol. 557, Mar. 2021, Art. no. 125993, doi: [10.1016/j.jcrysgro.2020.125993](https://doi.org/10.1016/j.jcrysgro.2020.125993).
- [56] E. Luna et al., "Interfacial intermixing in InAs/GaSb short-period-superlattices grown by molecular beam epitaxy," *Appl. Phys. Lett.*, vol. 96, no. 2, 2010, Art. no. 021904, doi: [10.1063/1.3291666](https://doi.org/10.1063/1.3291666).
- [57] E. Luna, R. Hey, and A. Trampert, "Interface properties of (In,Ga)As/GaAs quantum wells grown by solid-phase epitaxy," *J. Vac. Sci. Technol. B*, vol. 30, no. 2, 2012, Art. no. 02B108, doi: [10.1116/1.3672022](https://doi.org/10.1116/1.3672022).
- [58] E. G. Bithell and W. M. Stobbs, "Composition determination in the GaAs/(Al, Ga)As system using contrast in dark-field transmission electron microscope images," *Philos. Mag. A*, vol. 60, no. 1, pp. 39–62, 1989, doi: [10.1080/01418618908221178](https://doi.org/10.1080/01418618908221178).
- [59] E. Luna et al., "Interface properties of (Ga,In)(N,As) and (Ga,In)(As,Sb) materials systems grown by molecular beam epitaxy," *J. Cryst. Growth*, vol. 311, no. 7, pp. 1739–1744, Jun. 2009, doi: [10.1016/j.jcrysgro.2008.10.039](https://doi.org/10.1016/j.jcrysgro.2008.10.039).
- [60] X. Lü, E. Luna, L. Schrottke, K. Biermann, and H. T. Grahn, "Determination of the interface parameter in terahertz quantum-cascade laser structures based on transmission electron microscopy," *Appl. Phys. Lett.*, vol. 131, no. 17, Oct. 2018, Art. no. 172101, doi: [10.1063/1.5042326](https://doi.org/10.1063/1.5042326).
- [61] E. Luna, F. Ishikawa, P. D. Batista, and A. Trampert, "Indium distribution at the interfaces of (Ga,In)(N,As)/GaAs quantum wells," *Appl. Phys. Lett.*, vol. 92, no. 14, 2008, Art. no. 141913, doi: [10.1063/1.2907508](https://doi.org/10.1063/1.2907508).
- [62] E. Luna, Á. Guzmán, A. Trampert, and G. Álvarez, "Critical role of two-dimensional island-mediated growth on the formation of semiconductor heterointerfaces," *Phys. Rev. Lett.*, vol. 109, no. 12, 2012, Art. no. 126101, doi: [10.1103/PhysRevLett.109.126101](https://doi.org/10.1103/PhysRevLett.109.126101).
- [63] C. A. Curwen et al., "Thin THz QCL active regions for improved continuous-wave operating temperature," *AIP Adv.*, vol. 11, no. 12, Dec. 2021, Art. no. 125018, doi: [10.1063/5.0071953](https://doi.org/10.1063/5.0071953).
- [64] H. Richter et al., "4.7-THz local oscillator for the GREAT heterodyne spectrometer on SOFIA," *IEEE Trans. THz Sci. Technol.*, vol. 5, no. 4, pp. 539–545, Jul. 2015, doi: [10.1109/TTHZ.2015.2442155](https://doi.org/10.1109/TTHZ.2015.2442155).
- [65] X. Lü et al., "Terahertz quantum-cascade lasers for high-resolution absorption spectroscopy of atoms and ions in plasmas," *Semicond. Sci. Technol.*, vol. 38, no. 3, Jan. 2023, Art. no. 035003, doi: [10.1088/1361-6641/abclcd](https://doi.org/10.1088/1361-6641/abclcd).

- [66] J. Wubs et al., "Terahertz absorption spectroscopy for measuring atomic oxygen densities in plasmas," *Plasma Sources Sci. Technol.*, vol. 32, no. 2, Feb. 2023, Art. no. 025006, doi: [10.1088/1361-6595/acb815](https://doi.org/10.1088/1361-6595/acb815).
- [67] X. Lü, B. Röben, L. Schrottke, K. Biermann, and H. T. Grahn, "Correlation between frequency and location on the wafer for terahertz quantum-cascade lasers," *Semicond. Sci. Technol.*, vol. 36, no. 3, Mar. 2021, Art. no. 035012, doi: [10.1088/1361-6641/abdd4b](https://doi.org/10.1088/1361-6641/abdd4b).
- [68] B. Röben, X. Lü, K. Biermann, L. Schrottke, and H. T. Grahn, "Terahertz quantum-cascade lasers for high-resolution spectroscopy of sharp absorption lines," *J. Appl. Phys.*, vol. 125, no. 15, Apr. 2019, Art. no. 151613, doi: [10.1063/1.5079701](https://doi.org/10.1063/1.5079701).
- [69] L. Schrottke et al., "Intrinsic frequency tuning of terahertz quantum-cascade lasers," *J. Appl. Phys.*, vol. 123, no. 21, May 2018, Art. no. 213102, doi: [10.1063/1.5024480](https://doi.org/10.1063/1.5024480).
- [70] A. W. M. Lee, B. S. Williams, S. Kumar, Q. Hu, and J. L. Reno, "Tunable terahertz quantum cascade lasers with external gratings," *Opt. Lett.*, vol. 35, no. 7, pp. 910–912, Mar. 2010, doi: [10.1364/ol.35.000910](https://doi.org/10.1364/ol.35.000910).
- [71] C. A. Curwen, J. L. Reno, and B. S. Williams, "Terahertz quantum cascade VECSEL with watt-level output power," *Appl. Phys. Lett.*, vol. 113, no. 1, Jul. 2018, Art. no. 011104, doi: [10.1063/1.5033910](https://doi.org/10.1063/1.5033910).
- [72] N. Han et al., "Broadband all-electronically tunable MEMS terahertz quantum cascade lasers," *Opt. Lett.*, vol. 39, no. 12, pp. 3480–3483, Jun. 2014, doi: [10.1364/ol.39.003480](https://doi.org/10.1364/ol.39.003480).
- [73] I. Kundu et al., "Continuous frequency tuning with near constant output power in coupled Y-branched terahertz quantum cascade lasers with photonic lattice," *ACS Photon.*, vol. 5, no. 7, pp. 2912–2920, Jun. 2018, doi: [10.1021/acsp Photonics.8b00251](https://doi.org/10.1021/acsp Photonics.8b00251).
- [74] T. Alam et al., "Wideband, high-resolution terahertz spectroscopy by light-induced frequency tuning of quantum-cascade lasers," *Opt. Exp.*, vol. 27, no. 4, pp. 5420–5432, Feb. 2019, doi: [10.1364/OE.27.005420](https://doi.org/10.1364/OE.27.005420).
- [75] H. Richter et al., "A compact, continuous-wave terahertz source based on a quantum-cascade laser and a miniature cryocooler," *Opt. Exp.*, vol. 18, pp. 10177–10187, May 2010, doi: [10.1364/OE.18.010177](https://doi.org/10.1364/OE.18.010177).
- [76] A. Chopard et al., "Single-scan multiphase retrieval with a radiation of terahertz quantum cascade laser," *Appl. Phys. B-Lasers Opt.*, vol. 128, no. 3, Mar. 2022, Art. no. 63, doi: [10.1007/s00340-022-07787-x](https://doi.org/10.1007/s00340-022-07787-x).
- [77] X. Zheng, T. Gevart, and G. Gallot, "High precision dual-modulation differential terahertz ATR sensor for liquid measurements," *Opt. Lett.*, vol. 46, no. 16, pp. 4045–4048, Aug. 2021, doi: [10.1364/ol.430324](https://doi.org/10.1364/ol.430324).
- [78] F. Destic et al., "THz QCL-based active imaging dedicated to non-destructive testing of composite materials used in aeronautics," *Proc. SPIE*, vol. 7763, Aug. 2010, Art. no. 776304, doi: [10.1117/12.859247](https://doi.org/10.1117/12.859247).
- [79] J. R. Freeman, O. Marshall, H. E. Beere, and D. A. Ritchie, "Improved wall plug efficiency of a 1.9 THz quantum cascade laser by an automated design approach," *Appl. Phys. Lett.*, vol. 93, no. 19, Nov. 2008, Art. no. 191119, doi: [10.1063/1.3030881](https://doi.org/10.1063/1.3030881).
- [80] C. Walther, G. Scalari, J. Faist, H. Beere, and D. Ritchie, "Low frequency terahertz quantum cascade laser operating from 1.6 to 1.8 THz," *Appl. Phys. Lett.*, vol. 89, no. 23, Dec. 2006, Art. no. 231121, doi: [10.1063/1.2404598](https://doi.org/10.1063/1.2404598).
- [81] C. Worrall et al., "Continuous wave operation of a superlattice quantum cascade laser emitting at 2 THz," *Opt. Exp.*, vol. 14, no. 1, p. 171–181, 2006, doi: [10.1364/opeX.14.000171](https://doi.org/10.1364/opeX.14.000171).
- [82] L. Rezac et al., "First detection of the 63 μm atomic oxygen line in the thermosphere of Mars with GREAT/SOFIA," *Astron. Astrophys.*, vol. 580, Aug. 2015, Art. no. L10, doi: [10.1051/0004-6361/201526377](https://doi.org/10.1051/0004-6361/201526377).
- [83] H. Richter et al., "Direct measurements of atomic oxygen in the mesosphere and lower thermosphere using terahertz heterodyne spectroscopy," *Commun. Earth Environ.*, vol. 2, no. 1, Jan. 2021, Art. no. 19, doi: [10.1038/s43247-020-00084-5](https://doi.org/10.1038/s43247-020-00084-5).
- [84] M. Wienold et al., "OSAS-B: A 4.7-THz heterodyne spectrometer for atomic oxygen in the mesosphere and lower thermosphere," in *Proc. 48th Int. Conf. Infrared, Millimeter, Terahertz Waves*, 2023, pp. 1–2, doi: [10.1109/IRMMW-thz57677.2023.10299165](https://doi.org/10.1109/IRMMW-thz57677.2023.10299165).
- [85] M. Wienold et al., "OSAS-B: A balloon-borne terahertz spectrometer for atomic oxygen in the upper atmosphere," *IEEE Trans. THz Sci. Technol.*, vol. 14, no. 3, pp. 327–335, May 2024, doi: [10.1109/THZ.2024.3363135](https://doi.org/10.1109/THZ.2024.3363135).
- [86] M. G. Mlyneczek and S. Solomon, "A detailed evaluation of the heating efficiency in the middle atmosphere," *J. Geophys. Res. Atmos.*, vol. 98, no. D6, pp. 10517–10541, Jun. 1993, doi: [10.1029/93jd00315](https://doi.org/10.1029/93jd00315).
- [87] H.-W. Hübers et al., "Direct detection of atomic oxygen on the dayside and nightside of Venus," *Nature Commun.*, vol. 14, no. 1, Nov. 2023, Art. no. 6812, doi: [10.1038/s41467-023-42389-x](https://doi.org/10.1038/s41467-023-42389-x).
- [88] L. R. Zink, K. M. Evenson, F. Matsushima, T. Nelis, and R. L. Robinson, "Atomic oxygen fine-structure splittings with tunable far-infrared spectroscopy," *Astrophys. J.*, vol. 371, pp. L85–L86, Apr. 1991, doi: [10.1086/186008](https://doi.org/10.1086/186008).
- [89] K. Chance et al., "Pressure broadening of the 118.455 cm^{-1} rotational lines of OH by H₂, He, N₂, and O₂," *J. Mol. Spectrosc.*, vol. 146, no. 2, pp. 375–380, Apr. 1991, doi: [10.1016/0022-2852\(91\)90012-y](https://doi.org/10.1016/0022-2852(91)90012-y).
- [90] M. Wienold, T. Alam, L. Schrottke, H. T. Grahn, and H.-W. Hübers, "Doppler-free spectroscopy with a terahertz quantum-cascade laser," *Opt. Exp.*, vol. 26, no. 6, pp. 6692–6699, Mar. 2018, doi: [10.1364/OE.26.006692](https://doi.org/10.1364/OE.26.006692).
- [91] H. Pickett et al., "Submillimeter millimeter and microwave spectral line catalog," *J. Quant. Spectrosc. Radiat. Transf.*, vol. 60, no. 5, pp. 883–890, Nov. 1998, doi: [10.1016/s0022-4073\(98\)00091-0](https://doi.org/10.1016/s0022-4073(98)00091-0).
- [92] J. R. Wubs et al., "Validation of THz absorption spectroscopy by a comparison with ps-TALIF measurements of atomic oxygen densities," *Appl. Phys. Lett.*, vol. 123, no. 8, Aug. 2023, Art. no. 081107, doi: [10.1063/5.0160303](https://doi.org/10.1063/5.0160303).
- [93] J. R. Wubs et al., "Performance of a high-speed pyroelectric receiver as cryogen-free detector for terahertz absorption spectroscopy measurements," *Appl. Sci.*, vol. 14, no. 10, May 2024, Art. no. 3967, doi: [10.3390/app14103967](https://doi.org/10.3390/app14103967).



Xiang Lü received the master's degree in physics from Soochow University, Suzhou, China, in 2000, and the Ph.D. degree in physics from the Shanghai Institute of Technical Physics, Chinese Academy of Sciences, Shanghai, China, in 2003.

From 2003 to 2011, he was a Researcher with Shanghai Institute of Technical Physics, Chinese Academy of Sciences, working on modulated photoluminescence and photoreflectance spectroscopy. In 2011, he joined Paul-Drude-Institut für Festkörperelektronik, Berlin, Germany, where he is currently

a Senior Scientist working on the development of THz quantum-cascade lasers.



Benjamin Röben received the M.Sc. and doctoral degrees in physics from Technische Universität Berlin, Berlin, Germany, in 2014 and 2018, respectively.

From 2018 to 2021, he was a Scientist with Paul-Drude-Institut für Festkörperelektronik, Berlin, where his research was focused on the development of THz quantum-cascade lasers for spectroscopic applications. In 2021, he joined Physikalisch-Technische Bundesanstalt, Berlin, where his research interests include detector development, and THz time-domain and Fourier transform spectroscopy.



Valentino Pistore received the B.S. degree in physical engineering from the Politecnico di Torino, Turin, Italy, in 2014, the M.S. degree in nanotechnologies for ICTs from the Politecnico di Torino and the M.S. degree in quantum devices from Université Paris VII – Denis-Diderot, Paris, France, in 2016 as part of a double-degree program, and the Ph.D. degree in condensed matter physics from Sorbonne Université, Paris, in 2019.

He is currently a Postdoctoral Research Associate with Paul-Drude-Institut für Festkörperelektronik, Berlin, Germany, working on the development of THz quantum-cascade lasers.



Klaus Biermann received the diploma degree in physics from Friedrich-Alexander Universität, Erlangen-Nürnberg, Germany in 1998, and the doctoral degree in physics from Humboldt-Universität zu Berlin, Berlin, Germany, in 2007.

From 1998 to 2007, he was a Scientist with Heinrich-Hertz-Institut für Nachrichtentechnik and with Max-Born-Institut für Nichtlineare Optik und Kurzzeitspektroskopie, Berlin, Germany, where his research work was focused on molecular beam epitaxy (MBE) and femto-second spectroscopy of III-V semiconductor heterostructures with sub-ps response times, respectively. In 2007, he joined Paul-Drude-Institut für Festkörperelektronik, Berlin, where his research interests include MBE of GaAs-based structures and focusing on the growth on substrates of various crystal orientations, overgrowth of patterned templates, and closed-loop in situ control methods.



Esperanza Luna received the B.E. and M.S. degrees in physics (materials science) from the Universidad Complutense de Madrid, Madrid, Spain, in 1997, and the Ph.D. degree in physics from the Universidad Politécnica de Madrid, Madrid, in 2004.

In 2004, she joined Paul-Drude-Institut für Festkörperelektronik, Berlin, Germany, where she holds a Senior Scientist position since 2009. Her research focuses on the characterization by transmission electron microscopy techniques of semiconductor structures with a focus on the investigation of the interface properties.



Martin Wienold received the diploma and doctoral degrees in physics from Humboldt-Universität zu Berlin, Berlin Germany, in 2007 and 2012, respectively.

From 2008 to 2015, he was a Researcher with Paul-Drude-Institut für Festkörperelektronik, Berlin, on the development of terahertz quantum-cascade lasers. From 2015 to 2019, he was a Postdoctoral Fellow with Humboldt-Universität Berlin, working on terahertz imaging, and linear and nonlinear high-resolution spectroscopy. Since 2019, he has been a

Senior Scientist with Deutsches Zentrum für Luft und Raumfahrt (German Aerospace Center, DLR), Institute of Optical Sensor Systems, Berlin, working on terahertz heterodyne spectroscopy and instrumentation.



Heinz-Wilhelm Hübers received the diploma and doctoral degrees in physics from the Universität Bonn, Bonn, Germany, in 1991 and 1994, respectively.

From 1991 to 1994, he was with the Max-Planck Institut für Radioastronomie, Bonn. In 1994, he joined the Deutsches Zentrum für Luft und Raumfahrt (German Aerospace Center, DLR), Berlin, Germany, becoming the Head of Department in 2001. From 2009 to 2014, he has been a Professor of Experimental Physics with the Technische Universität Berlin and

the Head of the Department “Experimental Planetary Physics” with DLR. In 2014, he became the Director of the DLR-Institute of Optical Sensor Systems and a Professor of Physics with Humboldt-Universität zu Berlin. His research interests include THz physics and spectroscopy, particularly THz systems for astronomy, planetary research, and security.

Dr. Hübers was the recipient of the Innovation Award on Synchrotron Radiation in 2003, and the Lilienthal Award in 2007, and in 2021, an honorary doctorate at the Chalmers University of Technology, Gothenburg, Sweden.



Jente R. Wubs received the B.Sc. and M.Sc. degrees in applied physics from the Eindhoven University of Technology, Eindhoven, The Netherlands, in 2018 and 2020, respectively.

In 2021, she joined the Leibniz Institute for Plasma Science and Technology (INP), Greifswald, Germany, where she is currently a Doctoral Research Assistant working on the development, implementation, and validation of THz absorption spectroscopy for measuring atomic oxygen densities in plasmas.



Jean-Pierre H. van Helden received the M.Sc. and Ph.D. degrees in applied physics from the Eindhoven University of Technology, Eindhoven, The Netherlands, in 2001 and 2006, respectively.

From 2007 to 2012, he was a Postdoctoral Research Assistant with the Department of Chemistry, University of Oxford, working on laser spectroscopy of molecular gases and plasmas. In 2012, he joined the Leibniz Institute for Plasma Science and Technology (INP), Greifswald, Germany, where in 2017, he was appointed the Head of the Department of Plasma

Diagnostics. His research interests include the physicochemical processes in low and atmospheric pressure plasmas, particularly the development and application of laser-based diagnostics from UV to THz to characterize plasmas and their interactions with surfaces, and also on highly sensitive laser-based diagnostics using novel lasers in the mid- and far-infrared, including cavity-enhanced spectroscopy, frequency comb spectroscopy, and THz spectroscopy.



Pierre Gellie received the M.Sc. degree in applied physics from Université Paris 6—Pierre and Marie Curie, Paris, France, in 2008, and the Ph.D. degree in applied physics from Université Paris 7—Denis Diderot, Paris, in 2012.

From 2012 and 2015, he was a Postdoctoral Research Assistant with Université Paris 7 working on terahertz imaging and laser stabilization of THz quantum-cascade lasers. In 2015, he co-founded the company Lytid, and has acted as CTO since then.

With Lytid, his work is focused on the R&D and product development of scientific and industrial instrumentation using THz radiation. The core technologies are the THz quantum-cascade lasers, THz multiplied chains using Schottky diode circuits, and THz frequency-modulated continuous-wave radar systems based on GaAs and Si:Ge.



Lutz Schrottke received the diploma and doctoral degrees in experimental physics from Humboldt-Universität zu Berlin, Berlin, Germany, in 1983 and 1988, respectively.

From 1985 to 1991, he was with Zentralinstitut für Elektronenphysik, Berlin, working on thin-film electroluminescent devices. In 1992, he joined Paul-Drude-Institut für Festkörperelektronik, Berlin, as a scientific Staff Member. From 1995 to 1996, he was a Visiting Scholar with the Department of Physics, University of Michigan, Ann Arbor, MI, USA. His

research interests include THz quantum-cascade lasers as well as optical and transport properties of semiconductor heterostructures.